Local and chemical environment dependence of the magnetic properties of CoRh core-shell nanoparticles

L. E. Díaz-Sánchez,[1,2] J. Dorantes-Dávila,[3] and G. M. Pastor[1]

[1]*Institut für Theoretische Physik, Universität Kassel, Heinrich Plett Strasse 40, 34132 Kassel, Germany*

[2]*LCBMyN, Facultad de Ciencias, Universidad Autónoma del Estado de México, 50000 Toluca, Mexico*

[3]*Instituto de Física, Universidad Autónoma de San Luis Potosí, Alvaro Obregón 64, 78000 San Luis Potosí, Mexico*

(Received 24 February 2013; revised manuscript received 28 August 2013; published 24 October 2013)

The ground-state magnetic properties of Co_xRh_{1-x} nanoparticles having sizes in the range of 0.8–2 nm ($N = 43$ and 273 atoms) and Co concentrations $x \approx 0$, 0.25, 0.5, 0.75, and 1 are investigated in the framework of density-functional theory by using a fixed-moment method. Electron correlation effects are explored by comparing the results of the local spin-density and generalized-gradient approximations to the exchange and correlation functional. The role of chemical order on the magnetic behavior is investigated by considering a variety of core-shell atomic arrangements with nearly spherical CoRh interfaces. A local relaxation of the cluster geometry is performed by taking face-centered cubic structures as starting configurations. All considered Co_xRh_{1-x} clusters are found to be magnetic with an average spin moment per CoRh unit that is larger than in macroscopic alloys having similar concentrations. This is a consequence of both, the enhancement of the Co moments and the occurrence of important induced Rh moments, which couple parallel to the Co moments. The distribution of the local magnetic moments within the clusters is found to depend strongly on the local and chemical environment of the atoms. In particular, the Rh moments show a nontrivial dependence as a function of the distance to the CoRh interface. The results for the local magnetic moments are correlated to the electronic densities of states, which reflect the concentration and chemical-order dependence of the cluster electronic structure. Finally, the effects of coating and of the 3*d*-4*d* interface are analyzed by comparing the magnetic behaviors of core-shell particles with those of the corresponding pure Co and Rh cores.

DOI: 10.1103/PhysRevB.88.134423 PACS number(s): 36.40.Cg, 75.75.−c, 75.50.Cc, 73.22.−f

I. INTRODUCTION

Recent developments in nanostructure synthesis and characterization methods have opened novel possibilities to generate and manipulate small clusters and nanoparticles with controlled size and composition. A particularly intense research activity has been focused on the magnetism of transition metals (TMs) and their compounds, which are most intriguing from a fundamental perspective and important for a variety of technological applications.[1–5] Early experimental and theoretical investigations have been mainly devoted to monometallic TM nanoparticles.[6–9] In the case of pure Fe, Co, and Ni clusters, it is nowadays well understood how the large surface-to-volume ratio, the reduced local coordination, and the specific symmetry lead to an enhancement of the spin moments, orbital moments, and magnetic anisotropy energy as compared to the corresponding solids.[6,7,9–11] Moreover, the onset of ferromagnetism has been revealed in clusters of 4*d* or 5*d* elements, which are nonmagnetic in the bulk. This remarkable phenomenon, which is in fact most relevant for the present study, has been qualitatively predicted by theory[12] and subsequently observed experimentally in Rh_N clusters having 40–50 atoms[13] as well as in Pd nanoparticles having a diameter of about 6 nm.[14] Another important early discovery in this field is the central role played by the geometrical structure and local environment of the atoms on the electronic properties and magnetic order within the clusters.[7,9] Therefore, controlling the size and structure of the particles provides unique opportunities of manipulating the characteristics of new magnetic nanomaterials, which are not available in the macroscopic state.

More recently, the focus of attention in cluster magnetism has been progressively shifting to nanoscale alloys.[2–5,15–21] This is largely motivated by the prospects of tuning the chemical and physical properties by varying their composition, concentration, and chemical order. The study of binary magnetic clusters is particularly challenging, since it offers numerous ways of exploring competing ferromagnetic (FM), paramagnetic (PM), and antiferromagnetic (AF) behaviors. In this context, alloying a strongly FM 3*d* element (e.g., Fe, Co, or Ni) with highly spin-polarizable PM 4*d* or 5*d* atoms (e.g., Rh, Pd, Pt, etc.) deserves special attention. Indeed, besides the above-mentioned finite-size and surface effects, one usually observes very interesting proximity and interface effects which depend critically on the actual distribution of the different chemical species that are involved. A further important consequence of alloying is the possibility of inducing significant magnetic moments on otherwise PM 4*d* or 5*d* elements by introducing strongly ferromagnetic 3*d* atoms in their immediate local environment.[15–17] The magnetic response of the 4*d* or 5*d* clusters upon weak 3*d* doping is particularly strong. For example, the substitution of one nonmagnetic atom (e.g., Pd or Pt) by a magnetic impurity (e.g., Fe or Co) yields an enhancement of the cluster moment that goes well beyond, often more than doubling, the contribution of the magnetic impurity alone. Similar effects have been observed for magnetic impurities in 4*d* or 5*d* solids,[22] as well as for adatoms on surfaces.[22,23] Moreover, alloy clusters often show stable magnetic moments, which are much larger than those of bulk alloys with similar concentration.[15,16] For instance, experiments on CoRh nanoparticles indicate not only the presence of important Co moments, but also the development

of significant spin polarizations at the Rh atoms.[15] In addition, model calculations have shown a strong dependence of the magnetic order and magnetic anisotropy on the chemical order within the nanoalloys.[16,24] Still, systematic *ab initio* studies of CoRh clusters remain rather scarce.[25,26] It is the purpose of this paper to investigate the interplay between local environment, chemical order, and magnetism in CoRh nanoparticles in the framework of density-functional theory.

The remainder of the paper is organized as follows. The following section describes the theoretical method, computational parameters, and accuracy tests concerning the present study. Results for CoRh clusters having face-center-cubic-like core-shell structures are discussed in Sec. III. First, we consider clusters with $N = 43$ atoms. This corresponds approximately to the size where pure Rh_N clusters cease to be magnetic, so that the effects of Co doping should be particularly rich. Second, we focus on larger sizes ($N = 273$) which are close to the range of direct experimental interest. Finally, coating and interface effects are quantified by comparison with the corresponding pure core clusters. To conclude, Sec. IV summarizes the main results and points out some possible future implications.

II. COMPUTATIONAL DETAILS

The calculations are performed in the framework of Hohenberg-Kohn-Sham's density-functional theory[27] as implemented in the Vienna *ab initio* simulation package (VASP).[28–30] This computer program solves the spin-polarized Kohn-Sham (KS) equations at the scalar relativistic level in an augmented plane-wave basis set by using the projector augmented wave (PAW) method,[31] which is an efficient frozen atomic-core approximation. For $3d$ TMs, the electronic and magnetic properties are accurately described by considering the $3d$, $4s$, and $4p$ electrons as valence states. Exchange and correlation (XC) effects are treated within the spin-polarized local-density approximation (LDA)[32,33] and the generalized-gradient approximation (GGA).[34,35] The clusters are placed inside of a simple cubic supercell whose dimensions ensure that the interactions between neighboring images are negligible. In practice, this condition has been satisfied by separating the images by at least 15 Å. The KS wave functions are expanded in a plane-wave basis set with a kinetic-energy cutoff $E_{\max} = 230$ eV, which corresponds to Rh and is higher than the typically accepted value for Co ($E_{\max} = 170$ eV). These parameters guarantee that the total energy of the considered clusters is converged within 1 meV per atom or better. In metalliclike systems one often finds important changes in the level ordering close to the Fermi level as a function of the electronic density and cluster geometry used for defining the KS potential. This may lead to non-negligible changes in the orbital occupations and on the resulting spin-polarized density along the process of convergence of the self-consistent KS equations. Therefore, a smearing of the KS energy levels is introduced in order to improve numerical stability. We have used a Gaussian smearing method[36] with a mean-square deviation $\lambda \simeq 0.01$ eV. We have also verified that the total energy is nearly independent of the energy level smearing σ provided that it is not too large ($10 \leqslant \sigma \leqslant 50$ meV). This yields an energy due to entropy of about 1.0–1.5 meV, which is small enough for the purposes of this paper. As long as we are dealing with isolated clusters only the Γ point is considered in reciprocal space. In the case of the bulk the Monkhorst-Pack[37] grid is used. A number of tests have been performed in order to verify the accuracy of the present choice of calculation parameters, which are discussed at the end of this section.

In order to determine the ground-state magnetic and geometric configuration of the clusters, we apply the fixed spin-moment (FSM) method.[38] This procedure consists in performing independent self-consistent calculations for different fixed values of the z component of the total spin moment $S_z = N_\uparrow - N_\downarrow$, where N_σ stands for the number of electrons with spin σ. The value of S_z is then varied systematically in its full relevant range, from $S_z = 0$ to S_z slightly above the expected saturation values, until the lowest energy is obtained. The FSM density-functional calculations yield the lowest possible total energy for the given S_z within the framework of the considered approximation of exchange and correlation (e.g., the LDA or GGA).[38,39] Therefore, the value of S_z yielding the minimum energy corresponds to the total ground-state spin S of the given cluster structure.[40] A number of different spin configurations (typically 3–5) have been considered as starting points for solving the KS equations. These include ferromagnetic, antiferromagnetic, and more complex spin orders derived from self-consistent tight-binding (SCTB) d-band model calculations.[24] However, not all the proposed initial distributions of the local moments yield a self-consistent solution within VASP. In general we observe that starting with the spin moments obtained in SCTB studies, properly scaled to the actual value of S_z, is very useful in order to speed up convergence.

For each fixed S_z the cluster geometry is locally relaxed following the Hellmann-Feynman forces derived from the self-consistent spin-polarized density.[41,42] Equilibrium is assumed when the forces on all atoms are less than 10^{-3} eV/Å. The starting point of the structural relaxation are face-centered-cubic core-shell clusters with O_h symmetry, which are composed by a central atom and the successive shells of its nearest neighbors. CoRh clusters having up to $N = 273$ atoms have been considered. Although no constraints are imposed during the relaxations, the present procedure is not expected to yield a global optimum, since no systematic sampling of initial structures has been aimed. Nevertheless, we do observe local distortions with respect to the perfect O_h initial configuration. The equilibrium geometries have in most cases D_{4h} symmetry. The calculated changes in the interatomic distances amount to about 3%–5% in the alloy clusters, except for clusters doped with a single impurity at the center of symmetry, in which case they are below 1%. These distortions can be regarded as Jahn-Teller triggered, since the highest occupied KS orbital is degenerate in the O_h structures. However, notice that important rearrangements of the spin-polarized density, sometimes involving changes in the total moment, often occur along the relaxation process. The procedure involving scanning different S_z and relaxing the geometry is required in order to determine the most stable structure, total spin moment S, and the associated magnetic order, since the geometric, electronic, and magnetic degrees of freedom need to be treated on the same footing. Subsequently, the local magnetic moments μ_i are computed by integrating

TABLE I. Binding energy per atom E_b (eV), nearest neighbor (NN) distance d_{NN} (Å), and average spin moment per atom $\overline{\mu}$ (μ_B) of Co and Rh dimers and bulk as obtained by using the LDA and the GGA.

	E_b	d_{NN}	$\overline{\mu}$
Co_2 GGA	1.52	1.96	2.00
LDA	2.09	1.91	2.00
Expt. (Ref. 44)	1.72	2.31	2.00
Expt. (Ref. 45)	1.32	–	–
Rh_2 GGA	1.72	2.21	2.00
LDA	2.37	2.16	2.00
Co_{hcp} GGA	5.18	2.46	1.59
LDA	6.66	2.40	1.49
Expt. (Ref. 48)	–	2.51	1.58
Co_{fcc} GGA	5.16	2.47	1.61
LDA	6.63	2.41	1.54
Rh_{fcc} GGA	5.69	2.70	0.00
LDA	7.58	2.65	0.00
Expt. (Ref. 25)	5.75	2.69	0.00

the magnetization density inside the Wigner-Seitz (WS) sphere of each atom i.

In order to test the accuracy of our parameter choice we have calculated the binding energies, nearest neighbors distances, and magnetic moments of Co and Rh atoms, dimers and bulk. In the case of bulk we start with a k-point mesh $n_k = 10 \times 10 \times 10$ for hcp Co and $n_k = 10 \times 10 \times 16$ for fcc Co and Rh and then use the automatic generation of the k mesh by Monkhorst-Pack.[37] The results are compared with available experiments in Table I. For the energy calculations of the atoms, we use a fixed electronic configuration of $3d^8 4s^1$. For Co_2 and Rh_2 we obtain a spin moment per atom $\overline{\mu} = 2\,\mu_B$, which agrees with previous calculations and experiment.[43–46] Concerning the binding energies E_b, the LDA gives, as expected, an overbinding and an underestimation of the bond lengths (see Table I). However, E_b is smaller and thus closer to experiment when the GGA is considered. In fact, the results for the nearest neighbor (NN) distances and spin moments obtained in the GGA are in very good agreement with experiment and previous calculations.[46] Higher cut-off energies have also been considered up to $E_{max} = 500$ eV. Still, no significant changes in the magnetization values or in any other property presented in this work have been observed. This confirms the validity of our choice of technical parameters.

III. RESULTS AND DISCUSSION

The purpose of this section is to discuss the electronic and magnetic ground-state properties of Co_xRh_{1-x} nanoparticles. Emphasis is given to the the role of substitutions of Rh atoms by Co atoms in Rh_N for different size regimes, to the dependence of magnetic order and average magnetic moments on structure and chemical order, and to the correlation between magnetic order and local environment. First, we consider clusters having $N = 43$ atoms, which corresponds approximately to the size where pure Rh_N clusters cease to be magnetic. Thus, their magnetic behavior is expected to be particularly sensitive to Co substitution. Second, we focus on larger clusters having $N = 273$ atoms, which are close to the situation of experimental interest (diameter $\phi \simeq 1.5$ nm).[15] Finally, the effects of coating are analyzed by comparing the magnetic behavior of core-shell particles with that of pure Co and Rh clusters of the corresponding sizes. In this work we focus on spherical-like cluster surface with well-defined Co-Rh interfaces. However, other possible surface and interface shapes (e.g., cubo-octahedral-like) cannot be excluded, as suggested by some investigations in pure Rh_N clusters having $N \simeq 20$–60 atoms.[47]

A. CoRh clusters with $N = 43$ atoms

Previous first-principles calculations based on the local spin density approximation have shown that fcc-like Rh_{43} is paramagnetic or weakly ferromagnetic with nearly vanishing magnetic moments and a high magnetic susceptibility.[49,50] Therefore, CoRh clusters with $N = 43$ atoms are very interesting examples to analyze the dependence of the magnetic properties as a function of concentration and chemical order. Different fully segregated face centered cubic (fcc) structures having approximately spherical CoRh interfaces are considered as starting geometries for the structural relaxations. The corresponding relaxed structures are illustrated in Fig. 1 for representative values of the relative core size $\eta_c = N_c/N$, where N_c is the number of atoms in the core and N is the total number of atoms in the cluster. Co_nRh_m (Rh_nCo_m) refers to a cluster having an n-atom Co (Rh) core coated with m Rh (Co) atoms in the outer shells. After full local relaxation the cluster geometries show the D_{4h} point-group symmetry in all considered cases. It is interesting to analyze the stability of these nanoalloys by comparing the binding energy $E_b = [E(Co_nRh_m) - nE(Co) - mE(Rh)]/N$ as a function of composition, where E refers to the total energy of the corresponding cluster or atom. The calculations yield a monotonic increase of E_b with increasing Rh content: In the GGA, $E_b = 4.05$, 4.15, 4.28, and 4.31 eV for $Rh_{13}Co_{30}$, $Rh_{19}Co_{24}$, $Co_{19}Rh_{24}$, and $Co_{13}Rh_{30}$, respectively. This is

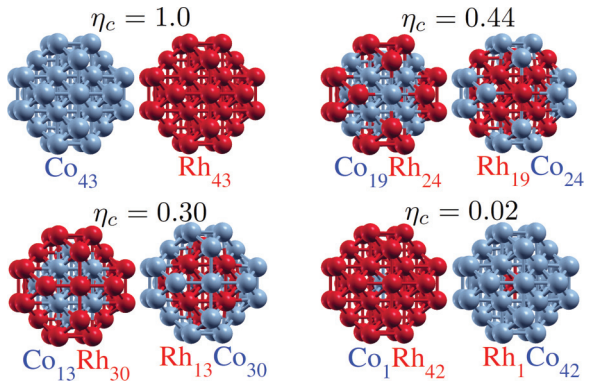

FIG. 1. (Color online) Illustration of the relaxed core-shell fcc-like structures of CoRh clusters having $N = 43$ atoms and different relative core sizes $\eta_c = N_c/N$, where N_c is the number of atoms in the core. Light (blue) balls represent Co atoms and dark (red) balls represent Rh atoms. The notation Co_nRh_m (Rh_nCo_m) designates a cluster having n Co atoms (Rh atoms) in the core and m Rh atoms (Co atoms) in the outer shell.

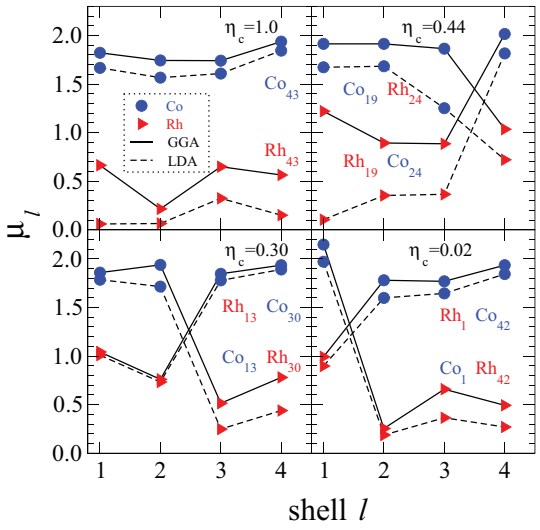

FIG. 2. (Color online) Local spin magnetic moments μ_l within the Wigner-Seitz spheres of the Co atoms (circles) and Rh atoms (triangles) in core-shell CoRh clusters having $N = 43$ atoms. Results are given for the average μ_l at each NN shell l surrounding the central atom $l = 1$. Co_nRh_m (Rh_nCo_m) designates a cluster having n Co atoms (Rh atoms) in the core and m Rh atoms (Co atoms) in the outer shell. The relative core sizes η_c are indicated in the insets. The lines connecting the points are a guide to the eye, where full (dashed) lines refer to the generalized-gradient (local-density) approximation. The corresponding relaxed cluster structures are illustrated in Fig. 1.

consistent with the fact that binding is stronger in Rh_{43} than in Co_{43} [$E_b(Rh_{43}) = 4.36$ eV, while $E_b(Co_{43}) = 3.96$ eV]. The same trend also holds in the solid.

As a result of the high symmetry of the relaxed geometries, the local DOS and the local magnetic moments are very similar for all the atoms i belonging to the same NN shell l of the central atom. Only small differences of the order of $5 \times 10^{-3}\ \mu_B$ are found in the local spin moments μ_i within any of these shells. Consequently, only the shell averages will be discussed in the text. Since for $N = 43$ there are four NN shells in the starting fcc geometry, we have eight different fully segregated core-shell arrangements. In the following we focus on these chemical orders, which correspond to the situation found in experiment when the dissociation times of the Co and Rh organometallic precursors are very different.[15]

In Fig. 2 the local magnetic moments in CoRh clusters with $N = 43$ atoms are shown as a function of the shell number l, where $l = 1$ corresponds to the central atom and $l = 4$ to the outermost shell. The results are obtained by integrating the spin density within the WS sphere of each atom. As already mentioned, only the shell averages μ_l are reported because the differences in the local moments within a shell are very small. This figure, together with Table II, where various average moments are summarized, contains a wealth of information on the magnetic order and on surface, interface, and doping effects. Let us first discuss the results for pure clusters, which are the reference for analyzing the behavior of the alloys.

In Co_{43} the average magnetic moment per atom $\bar{\mu} = 1.93\ \mu_B$ in the GGA is about 20% larger than the bulk ground-state spin magnetization (see Tables I and II). This enhancement is dominated by the contribution of the outermost

TABLE II. Average spin magnetic moments in core-shell Co_nRh_m clusters having $N = n + m = 43$ atoms as obtained by using the GGA approximation. Results are given for the total spin moment per atom $\bar{\mu} = (\nu_\uparrow^T - \nu_\downarrow^T)/N$, the average moment within the Wigner-Seitz (WS) spheres $\bar{\mu}^{WS} = (\sum_{i=1}^{N} \mu_i)/N$, the average Rh moment $\bar{\mu}_{Rh}^{WS} = (\sum_{i=1}^{m} \mu_i)/m$, and the average Co moment $\bar{\mu}_{Co}^{WS} = (\sum_{i=1}^{n} \mu_i)/n$. The values in brackets are the corresponding d-electron contributions.

	$\bar{\mu}$	$\bar{\mu}^{WS}$	$\bar{\mu}_{Rh}^{WS}$	$\bar{\mu}_{Co}^{WS}$
Rh_{43}	0.54	0.48	0.48	
		(0.47)	(0.47)	
$Rh_{19}Co_{24}$	1.61	1.53	0.91	2.02
		(1.52)	(0.93)	(1.99)
$Rh_{13}Co_{30}$	1.63	1.57	0.78	1.93
		(1.58)	(0.83)	(1.91)
Rh_1Co_{42}	1.93	1.85	0.99	1.87
		(1.85)	(1.01)	(1.87)
Co_{43}	1.93	1.85		1.85
		(1.86)		(1.86)
Rh_{43}	0.54	0.48	0.48	
		(0.47)	(0.47)	
Co_1Rh_{42}	0.54	0.49	0.45	2.15
		(0.48)	(0.44)	(2.14)
$Co_{13}Rh_{30}$	1.14	1.09	0.73	1.93
		(1.10)	(0.72)	(1.96)
$Co_{19}Rh_{24}$	1.47	1.42	1.04	1.90
		(1.44)	(1.04)	(1.94)
Co_{43}	1.93	1.85		1.85
		(1.86)		(1.86)

shell $l = 4$, which can be understood as a consequence of the reduced local coordination number $z_4 = 5$ and the associated reduction of the effective d-band width.[9] It should be, however, noted that the coordination number $z_3 = 8$ at the $l = 3$ shell is also smaller than in the bulk. The local moments μ_l are in fact larger than the bulk magnetization for all l. Comparing the GGA and LDA results for Co_{43} one observes pretty much the same trends, just the LDA yields somewhat smaller local moments than the GGA. This behavior is common to all sizes and compositions. It reflects the usual tendency of the LDA to overestimate electron delocalization and chemical binding. Consequently, the effective d-band width is larger in the LDA and the local and average magnetic moments are smaller.

In the case of Rh_{43} the local magnetic moments are clearly smaller than in Co_{43}. Nevertheless, the enhancement with respect to the nonmagnetic solid is much more significant. Notice that in Rh_{43} the local moments $\mu_l \simeq (0.3\text{–}0.7)\ \mu_B$ are far from saturated, even in the GGA. The actual number of d electrons is $\nu_d \simeq 8$, which implies saturation for $\mu_{sat} \simeq (10 - \nu_d)\ \mu_B \simeq 2\ \mu_B$. This explains the richer environment dependence of μ_l showing oscillations as we move from the center to the surface of the cluster. The amplitude of the variations of μ_l, as well as the average values, are more important in the GGA than in the LDA. The details of the XC functional are particularly important at the central atom $l = 1$ of Rh-rich clusters (e.g., Rh_{43} and $Rh_{19}Co_{24}$). Here the GGA predicts larger local moments than for the surrounding shells, in contrast to the LDA (see Fig. 2 for $\eta_c = 1.0$ and 0.44). These results are not a simple consequence of differences in LDA and

GGA interatomic distances. They rather reflect different ways of treating the subtle XC contributions.

In order to put apart the XC effects on the d electrons responsible for magnetism, from the XC effects on the chemical binding and on the resulting equilibrium interatomic distances, we have performed GGA calculations by using the equilibrium positions derived in the LDA and vice versa. For simplicity, we consider perfect fcc-like Rh_{43} clusters with NN distances equal to $d_{\mathrm{LDA}} = 2.62$ Å and $d_{\mathrm{GGA}} = 2.69$ Å, which are the LDA and GGA equilibrium distances between the central atom and its NNs after relaxation. It turns out that such changes in the NN distances do not affect the value of the local magnetic moment at the central atom, neither in the LDA nor in the GGA. The differences in μ_1 for the two considered distances is only $\Delta\mu_1^{\mathrm{LDA}} \simeq \Delta\mu_1^{\mathrm{GGA}} \simeq 0.01$–$0.02\ \mu_B$. Even at the cluster surface, where the differences in the interatomic distance often have a stronger influence on μ_l one obtains the same trend ($\Delta\mu_4^{\mathrm{LDA}} \simeq \Delta\mu_4^{\mathrm{GGA}} \simeq 0.01$–$0.02\ \mu_B$). One concludes that the magnetization profile μ_l versus l of Rh-rich clusters is particularly sensitive to electronic correlations.

Quantitatively, it is the LDA with an average magnetic moment per atom $\bar{\mu}_{43}^{\mathrm{LDA}} = 0.16\ \mu_B$ the one that comes closest to the experimental result $\bar{\mu}_{43}^{\mathrm{Expt}} = (0.16 \pm 0.13)\ \mu_B$ derived from Stern-Gerlach deflection measurements.[13] The GGA yields $\bar{\mu}_{43}^{\mathrm{GGA}} = 0.54\ \mu_B$. At this stage it is important to remark that our results differ significantly from the calculations by Li *et al.*,[49,50] who reported a vanishing spin polarization in Rh_{43}. In order to understand the source of this discrepancy we have recalculated the magnetic properties of Rh_{43} by using the same energy-level smearing $\lambda = 0.4$ eV as in Refs. 49 and 50. In this case we also obtain a nonmagnetic solution. This shows that the numerical stability of the results in the limit of $\lambda \to 0$ needs to be checked with care, particularly when one obtains a nonmagnetic state after choosing relatively large values of λ (e.g., $\lambda/k_B \simeq 4000$ K). In fact, using $\lambda = 0.01$ eV as in the present work, or even $\lambda = 0.05$ eV, yields a magnetic ground state for Rh_{43} both in the LDA and GGA.

In order to discuss the properties of the alloys it is most interesting to start from the highly spin-polarizable pure Rh clusters and analyze the effects of replacing progressively Rh by Co. We consider first the case where Rh is in the core. As a result of the substitution of the outer shell by Co atoms one obtains the cluster $Rh_{19}Co_{24}$, which shows an important enhancement of μ_l at all Rh atoms (see Fig. 2). The Co moments (outermost shell) are also slightly larger than in pure Co_{43}. This is probably related to a slight increase in the number of d holes at the Co atoms in contact with Rh. The enhancement of the average magnetic moment per atom—from $\bar{\mu} = 0.54\ \mu_B$ in Rh_{43} to $\bar{\mu} = 1.61\ \mu_B$ in $Rh_{19}Co_{24}$ (see Table II)—is not only due to the larger Co contributions ($\bar{\mu}_{\mathrm{Co}}^{\mathrm{WS}} = 2.02\ \mu_B$). The enhancement of the Rh local moments is equally important. In fact, $\bar{\mu}_{\mathrm{Rh}}^{\mathrm{WS}} = 0.48\mu_B$ in Rh_{43}, while $\bar{\mu}_{\mathrm{Rh}}^{\mathrm{WS}} = 0.91\ \mu_B$ in $Rh_{19}Co_{24}$ (see Table II). This demonstrates the remarkably high spin polarizability of Rh clusters in this size range.

A further increase of the Co content in $Rh_{13}Co_{30}$ does not yield a very significant change in the local Rh moments calculated in the GGA. Actually a small reduction of μ_l^{Rh} is observed. However, the LDA results for μ_l^{Rh} are significantly enhanced, now becoming very similar to the GGA ones (see Fig. 2 for $\eta_c = 0.30$). The average magnetic moments per atom in $Rh_{13}Co_{30}$ is nearly the same as in $Rh_{19}Co_{24}$. This is the result of a compensation between a larger contribution of Co atoms and a small reduction of the Rh local moments (see Table II). Finally, for very high Co content as in Rh Co_{42} ($\eta_c = 0.02$) we recover a magnetization profile which is very similar to pure Co_{43}, as far as the Co shells are concerned. The local moment $\mu_1^{\mathrm{Rh}} = 0.99\ \mu_B$ at the central Rh atom in $RhCo_{42}$ and in $Rh_{13}Co_{30}$ are very similar.

Co substitution at the cluster core, which we denote by Co_nRh_m, yields a qualitatively different behavior. In this case we observe a nonmonotonous dependence of the Rh spin polarization with increasing Co content: $\bar{\mu}_{\mathrm{Rh}}^{\mathrm{WS}} = 0.48$, 0.45, 0.73, and $1.04\ \mu_B$ in Co_nRh_{43-n} for $n = 0$, 1, 13, 19, respectively. Even in the very dilute limit (e.g., $CoRh_{42}$) the Co spin moments are strong ($\bar{\mu}_{\mathrm{Co}}^{\mathrm{WS}} \simeq 2\ \mu_B$). Interestingly, $\bar{\mu}_{\mathrm{Co}}^{\mathrm{WS}}$ tends to decrease with increasing Co concentration. This suggests that the enhancement of $\bar{\mu}_{\mathrm{Co}}^{\mathrm{WS}}$ is not due to a reduction of the local coordination numbers—the Co atoms are in the core—but rather to a small charge transfer from Co to Rh, which causes an increase in the number of polarizable $3d$ holes at the Co atoms. Similar $3d$ to $4d$ charge transfers have been found in FeRh clusters.[51]

Concerning the spatial distribution of the spin polarization, we observe that more than 95% of the total magnetization originates in the WS spheres of the atoms, when the Co content is important. This can be verified by comparing the results for $\bar{\mu}$ and $\bar{\mu}^{\mathrm{WS}}$ in the Table II. Notice that in the Rh rich limit (e.g., in Rh_{43} and Co_1Rh_{42}) the local contribution drops to about 90%. This reflects a more important spill-off of the spin-polarized density, although the local atomic contributions remain largely dominant. Comparing d and sp moments within the WS spheres we observe, as expected, that the latter are quite small. In most cases the sp moments are parallel to the d moments. However, when Rh is at the core (e.g., in $Rh_{19}Co_{24}$ and $Rh_{13}Co_{30}$) we find an appreciable antiparallel sp polarization $\mu_{sp}^{\mathrm{Rh}} \simeq -(0.02$–$0.05)\ \mu_B$ at the Rh atoms. Antiparallel sp moments are also found at the Co atoms of some clusters having a Co core (e.g., in $Co_{13}Rh_{24}$). This effect could be investigated experimentally by performing Knight-shift measurements.

The spin-polarized density of states (DOS) $\rho_\sigma(\varepsilon)$ provides a further insight on the electronic structure and magnetic properties of $3d$-$4d$ nanoalloys as a function of composition and chemical order. Figure 3 shows the DOS derived from the Kohn-Sham spectrum within the GGA approximation for the core-shell CoRh clusters illustrated in Fig. 1. For the sake of comparison, the contrasting behaviors of pure Co and Rh clusters are considered first. In the case of Co_{43}, the DOS reflects clearly the strong ferromagnetic order within the cluster. A large exchange splitting and an almost fully occupied majority band are found. In contrast, the DOS of Rh_{43} shows a nonsaturated weak ferromagnetic behavior with nonvanishing DOS at the Fermi energy ε_F for both spin directions. In all cases the electronic structure near ε_F is dominated by the d-electron contributions. However, the d-band width is much narrower in Co than in Rh, particularly for the majority states.

As a function of concentration, the DOS reflects the crossover between the previous contrasting behaviors. For

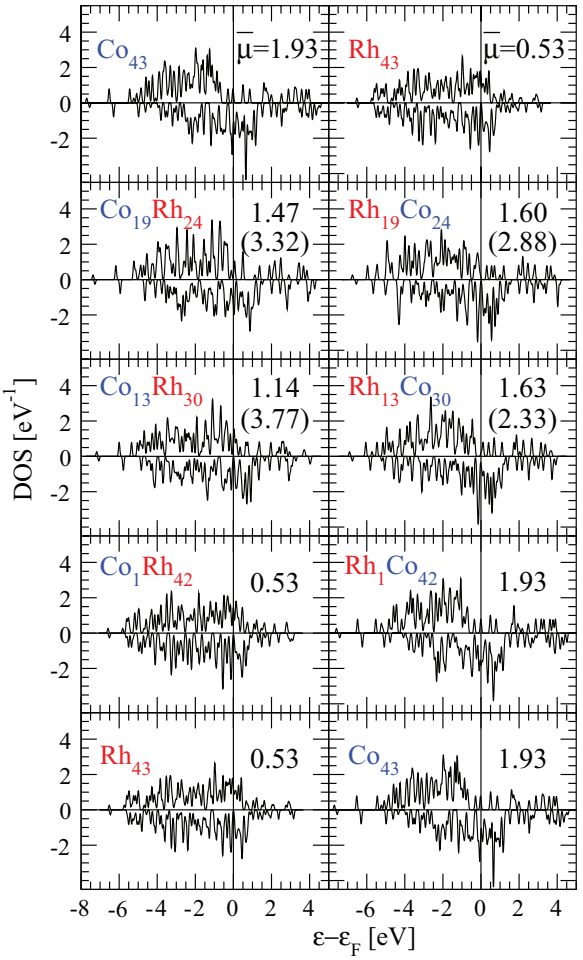

FIG. 3. (Color online) Spin-polarized average density of states (DOS) of core-shell Co_nRh_m clusters having $N = n + m = 43$ atoms as a function of the Kohn-Sham energy ε relative to the Fermi energy ε_F. Positive (negative) values refer to results for majority (minority) spin as obtained in the GGA. The corresponding average magnetic moments per atom $\overline{\mu} = (\nu_\uparrow^T - \nu_\downarrow^T)/N$ are indicated, together with the average magnetic moment per Co atom $\bar{\mu}_{\rm Co}^{\rm WS} = (\sum_{i=1}^{m+n} \mu_i)/n$ in brackets. The left-side (right-side) plots refer to clusters having a Co (Rh) core surrounded by a Rh (Co) outer shell. The underlying relaxed geometries are illustrated in Fig. 1.

example, starting from pure Co clusters and increasing the Rh content (left column), one observes a progressive increase of the d-band width for both spin directions. The upper bound of the majority-spin d DOS increases and comes closer to ε_F (see, for example, the results for Rh_1Co_{42} and $Rh_{13}Co_{30}$ in Fig. 3). Finally, for large enough Rh content, the majority-spin DOS is no longer zero at ε_F, which corresponds to nonsaturated magnetic moments (see, for example, the DOS of $Rh_{19}Co_{24}$ and $Co_{19}Rh_{24}$). Qualitatively, the trends are similar for both types of core-shell chemical orders.

B. CoRh clusters with $N = 273$ atoms

In this section we discuss the magnetic properties of larger alloy clusters, which diameter $\phi \simeq 1.5$ nm is close to those obtained by means organometallic chemistry or low-energy cluster-beam deposition methods.[3,5,15] Motivated by the

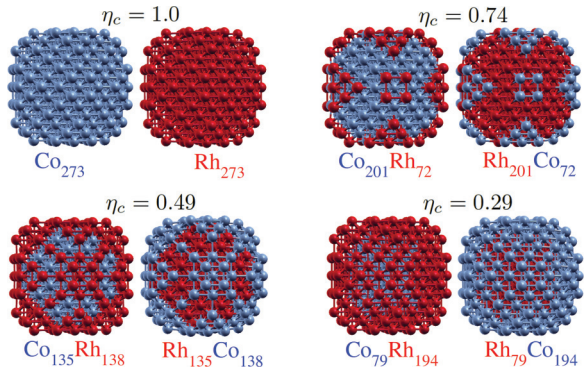

FIG. 4. (Color online) Illustration of the relaxed core-shell fcc-like structures of CoRh clusters having $N = 273$ atoms and different relative core sizes $\eta_c = N_c/N$, where N_c is the number of atoms in the core. Light (blue) balls represent Co atoms and dark (red) balls represent Rh atoms. Co_nRh_m (Rh_nCo_m) designates a cluster having n Co atoms (Rh atoms) in the core and m Rh atoms (Co atoms) in the outer shell.

results of experiment and simulations,[52] we consider fcc-like structures with segregated core-shell Co and Rh components, as the starting configurations of the unconstrained local geometry optimizations. The structures considered for the actual calculations contain a central atom and the successive shells of its closest 15 NNs, which yields $N = 273$ atoms in all. Exploring this size range is particularly interesting, since Rh and Co cluster are magnetically very different here. While Co_N is expected to remain ferromagnetic all along its way to the bulk, Rh_{273} is expected to be nonmagnetic or weakly magnetic. Still, the latter should preserve a large magnetic susceptibility, as a result of which very interesting magnetic behaviors could be triggered by Co doping. The optimized structures of CoRh nanoparticles with $N = 273$ atoms are illustrated in Fig. 4. As before, Co_nRh_m (Rh_nCo_m) refers to clusters having n Co atoms (Rh atoms) in the core and m Rh atoms (Co atoms) in the outer shells ($N = n + m$). The results for the magnetic properties are summarized in Fig. 5 and Table III for representative values of the relative core sizes η_c.

In the case of pure Co_{273} the local spin moment μ_1 at the central atom is somewhat smaller than the bulk one $\mu_1 \simeq 1.5\ \mu_B$, while the calculated $\mu_b = 1.59\ \mu_B$. As we move away from the cluster center towards the surface, the Co moments increase up to $\mu_l \simeq 1.9\ \mu_B$ for $l = 14$ and 15 showing very weak oscillations (see Fig. 5). The LDA moments are in general smaller than the GGA ones. Note that in pure Rh clusters the local spin moments are very small. They present some oscillations as a function of the shell number l showing no sign of antiferromagnetic order. Only at the surface the local moments are significant: $\mu_l \simeq 0.5\ \mu_B$ for $l = 13$ and 15. This yields a very small average magnetic moment per atom $\bar{\mu}$ (see Table III).

In the case of nanoalloys having a Co core and a Rh outer shell, the magnetic moments at the innermost Co atoms are similar to those found in pure Co_N. They increase as one goes from the center to the CoRh interface, except when the Co core is small. For example, in $Co_{79}Rh_{194}$ one observes that μ_l(Co) is nearly constant or tends to decrease with increasing l. Significant magnetic moments are induced in the Rh atoms

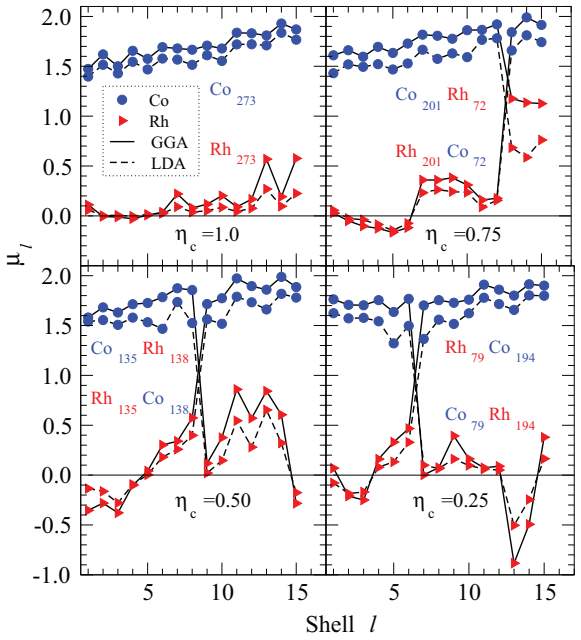

FIG. 5. (Color online) Local spin magnetic moments μ_l within the Wigner-Seitz spheres of the Co atoms (circles) and Rh atoms (triangles) in core-shell CoRh clusters having $N = 273$ atoms. Results are given for the average μ_l at each NN shell l surrounding the central atom $l = 1$. Co_nRh_m (Rh_nCo_m) designates a cluster having n Co atoms (Rh atoms) in the core and m Rh atoms (Co atoms) in the outer shell. The relative core sizes η_c are indicated in the insets. The lines connecting the points are a guide to the eye, where full (dashed) lines refer to the generalized-gradient (local-density) approximation. The corresponding relaxed cluster structures are illustrated in Fig. 4.

TABLE III. Average spin magnetic moments in core-shell Co_nRh_m clusters having $N = n + m = 273$ atoms. Results are given for the total spin moment per atom $\bar{\mu}$, the average moment within the Wigner-Seitz (WS) spheres $\bar{\mu}^{WS}$, the Rh average moment μ_{Rh}^{WS}, and the average Co moment μ_{Co}^{WS} as in Table II.

	$\bar{\mu}$	$\bar{\mu}^{WS}$	$\bar{\mu}_{Rh}^{WS}$	$\bar{\mu}_{Co}^{WS}$
Rh_{273}	0.19	0.18	0.18	
		(0.18)	(0.18)	
$Rh_{201}Co_{72}$	0.62	0.60	0.13	1.92
		(0.61)	(0.14)	(1.91)
$Rh_{135}Co_{138}$	1.07	1.06	0.22	1.88
		(1.07)	(0.24)	(1.89)
$Rh_{79}Co_{194}$	1.36	1.35	0.19	1.82
		(1.37)	(0.21)	(1.84)
Co_{273}	1.75	1.74		1.74
		(1.77)		(1.77)
Rh_{273}	0.19	0.18	0.18	
		(0.18)	(0.18)	
$Co_{79}Rh_{194}$	0.45	0.46	−0.06	1.74
		(0.48)	(−0.05)	(1.78)
$Co_{135}Rh_{138}$	1.12	1.11	0.45	1.78
		(1.13)	(0.45)	(1.82)
$Co_{201}Rh_{72}$	1.65	1.61	1.15	1.78
		(1.64)	(1.13)	(1.83)
Co_{273}	1.75	1.74		1.74
		(1.77)		(1.77)

surrounding the spin-polarized Co core, the behavior of which depends remarkably on the thickness of the coating Rh shell. In $Co_{201}Rh_{72}$ one observes that surface and interface effects, i.e., reduced coordination number and proximity to the Co atoms, combine to yield very important local moments at the thin Rh outer shell [μ_l(Rh) $\simeq 1.1\ \mu_B$ for $l = 13$–15]. These align parallel to the Co moments yielding a significant contribution to the average magnetization $\bar{\mu}$. For thicker Rh outer shells (e.g., $Co_{135}Rh_{138}$ and $Co_{79}Rh_{194}$) the spin moments induced at the Rh interface atoms are very small. This is in partly due to a d-electron charge transfer, about 0.1–0.2 minority electrons per atom from Co to Rh at the interface, which reduces (increases) the number of d holes and the local moments at the Rh (Co) atoms. As we move away from the CoRh interface towards the surface (larger l in Fig. 5) the Rh spin polarization increases showing important oscillations and changes of sign. This reflects a tendency to AF coupling, which is characteristic of low-spin states. For Rh-rich content, small Co core, the reduction of the Co moments at the interface is not compensated by the tiny induced Rh moments (see, for example, $Co_{79}Rh_{194}$). Consequently, not only the average moment per atom $\bar{\mu} = 0.45\ \mu_B$ is small, but also the average magnetization per Co atom $\bar{\mu}_{Co}^{WS} = 1.74\ \mu_B$ is smaller than in the other cases.

The calculated average magnetic moments per Co atom $\bar{\mu}_{Co}^{WS} = (\sum_{i=1}^{m+n} \mu_i)/n$ in these nanoalloys are very similar, regardless of the type of core-shell arrangement. This holds as long as the number of Rh atoms is comparable and the Rh content is not very large. However, the magnetization profiles, i.e., the distributions of the spin-polarized density μ_l(Rh) as a function of l, are most sensitive to the chemical order (see Fig. 5). In the case of Rh-core nanoparticles, the Co moments are largest at the cluster surface ($9 \leqslant l \leqslant 15$) and decrease slightly at the CoRh interface. The induced Rh moments are quite significant, in particular at the interface [μ_l(Rh) $\simeq 0.4$–$0.5\ \mu_B$] where they couple parallel to the Co moments. In addition, important oscillations and changes of sign of μ_l(Rh) are observed as one moves away from the interface towards the cluster center. This AF-like order, combined with the increase of the Co moments, yields average magnetic moments per atom which are similar to those of the previously discussed Co-core case. Finally, concerning the role of electronic correlations, it is worth noting that the LDA and GGA give very similar qualitative behaviors for all considered alloy clusters. This is remarkable taking into account the wide variety of magnetization profiles reported in Fig. 5. The main difference is the already mentioned systematic tendency of the LDA to underestimate the absolute value of μ_l. Nevertheless, the predicted magnetic order coincides with the GGA.

The density of states provides detailed information on the local and chemical environment dependence of the electronic structure of nanoalloys, in particular concerning the hybridizations between Co and Rh states and the resulting proximity effects. In Fig. 6 results are given for the GGA Kohn-Sham single-particle DOS of CoRh clusters having $N = 273$ atoms and representative values of the Co-Rh content. For the sake of comparison, results for bulk Rh and Co are also shown. The DOS of pure Co_{273} presents the FM-like exchange splitting that is characteristic of a parallel alignment of the Co moments within the cluster. Already at these sizes the cluster DOS shares

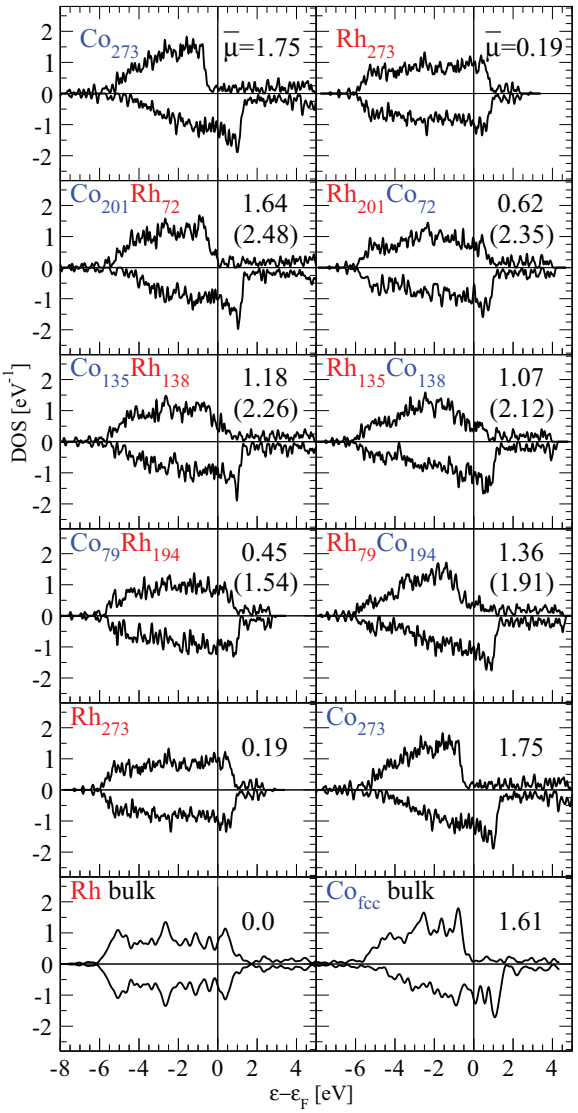

FIG. 6. (Color online) Spin-polarized average density of states (DOS) of core-shell Co_nRh_m clusters having $N = n + m = 273$ atoms as a function of the Kohn-Sham energy ε relative to the Fermi energy ε_F. Positive (negative) values refer to majority (minority) spin. The corresponding average spin moments per atom $\overline{\mu} = (\nu_\uparrow^T - \nu_\downarrow^T)/N$ are indicated together with the average local moment per Co atom $\bar{\mu}_{\rm Co}^{\rm WS} = (\sum_{i=1}^{m+n} \mu_i)/n$ in brackets. The left-side (right-side) plots correspond to clusters having a Co (Rh) core surrounded by a Rh (Co) shell. The underlying relaxed geometries are illustrated in Fig. 4.

a number of features with the bulk DOS (see Fig. 6). However, notice that the most remarkable narrow peaks in the bulk DOS, a consequence of specific features in the band structure of the periodic solid, are absent from the finite clusters. In Rh_{273} the DOS is very similar for both spin projections, as expected for a weakly magnetic system [$\overline{\mu}(Rh_{273}) = 0.19\ \mu_B$]. Some similarities with the bulk DOS are observed, although the cluster bandwidth is still appreciably narrower. The contrasting results for the pure Co and Rh clusters lets us expect an interesting dependence as a function of concentration.

In the CoRh nanoalloys significant spin moments are induced at the Rh atoms. As a result, exchange splittings appear in the local Rh DOS. This is clearly seen in $Rh_{201}Co_{72}$ and $Co_{79}Rh_{194}$ (see Fig. 6). The induced Rh spin moments align parallel to the total cluster magnetization and thus increase the average moment per Co atom $\bar{\mu}_{\rm Co}$, except when the Co core is small (e.g., $Co_{79}Rh_{194}$). See the values in brackets in the insets of Fig. 6. For nearly equal Co and Rh concentrations the DOS shows very interesting features, which reflect characteristics of both components. Notice, for example, the peak in the minority-spin DOS of $Co_{135}Rh_{138}$ above ε_F, which is similar to one found in Co_{273}. Moreover, the Co-Rh hybridizations yield a d-band width which is similar to that of Rh_{273}. And yet, a non-negligible exchange splitting is present. Qualitatively, the electronic structure of the nanoalloys reflects the remarkable crossover between strongly ferromagnetic and almost nonmagnetic behaviors as a function of compositions.

C. Coating and surface effects

The effects of coating and $3d$-$4d$ interfaces may be quantified by comparing the results of core-shell nanoparticles with those of the corresponding pure Co and Rh cores, as obtained by removing the outer shells. This provides a complementary perspective to interface magnetism in nanoalloys, in particular concerning the environment dependence of the induced local moments. In Fig. 7 the local spin moments μ_l at the different shells l of coated and uncoated clusters are compared. The

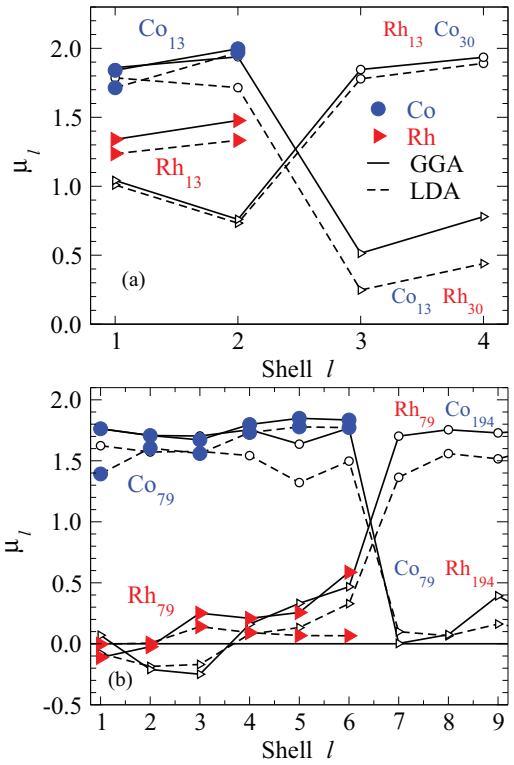

FIG. 7. (Color online) Comparison between the magnetization profiles of pure (full symbols) and coated (open symbols) clusters: (a) Pure Co_{13}, Rh-coated $Co_{13}Rh_{30}$, pure Rh_{13}, and Co-coated $Rh_{13}Co_{30}$, and (b) pure Co_{79}, Rh-coated $Co_{79}Rh_{194}$, pure Rh_{79}, and Co-coated $Rh_{79}Co_{194}$. Results are given for the local spin moments μ_l within the WS spheres of the atoms at the NN shells l surrounding the central atom $l = 1$. Full (dashed) lines refer to the GGA (LDA).

core sizes $N_c = 13$ and 79 are considered as representative examples.

In the case of Co cores, the GGA results for the Co spin moments are rather insensitive to the presence or not of the outer Rh shells. Instead, the LDA moments tend to decrease at the interface Co atoms in contact with Rh, particularly for the smaller core size $N_c = 13$. These differences appear to reflect strong Co-Rh hybridizations leading to weaker magnetism, which is not unusual in the LDA. At the Rh side of the interface one finds a different magnetic behavior than at the Co side, since the Rh spin moments are almost vanishing. The quenching of Rh moments is probably favored by hybridization and charge-transfer effects, typically 0.1 electrons per atom, which tend to enhance the number of polarizable d holes in Co at the expense of Rh holes. In addition, the curvature of the interface should play a role, as already observed in self-consistent tight-binding calculations.[24]

In Rh-core nanoparticles a different trend is observed. In this case, the Rh moments at the interface are more important and the charge transfer between Co an Rh atoms is much weaker (typically 0.02 electrons per atom). The magnetic susceptibility of the Rh atoms, which is triggered by the proximity with Co, dominates over charge transfer effects. Thus, stronger Rh spin polarizations are favored. For the larger core size $N_c = 79$, the Rh local moments μ_l show stronger oscillations and changes of sign inside the core, when the Co coating is present. In other words, for the same Rh-cluster size, the Rh surface favors ferromagnetic order more strongly than a Co-Rh interface.

The role of chemical order on the magnetic properties of the different CoRh interfaces can be qualitatively understood by contrasting their specific local atomic environments. In the first case (Co core and Rh shell) all Co atoms have a bulklike coordination number with less Co than Rh NNs at the interface. This increases the effective local d-band width at the Co interface atoms, which tends to reduce the local Co moments. This effect, particularly clear in the LDA results, is actually compensated to some extent by an increase of the number Co $3d$ holes. Furthermore, the interface Rh atoms have few Co NN, so that the induced Rh polarization is quite small. Finally, the curvature at the surface of the larger particles is not enough to sustain the formation of large local Rh moments. In contrast, in the second case (Rh core and Co shell) there are several factors that enhance magnetism. First, the reduction in coordination number at the surface Co atoms increases the local spin moments. Second, the interface Co atoms, being outside, have more Co than Rh NNs, so that the Rh-induced additional d-band broadening is weaker. Finally, the Rh atoms at the interface have now a majority of strongly magnetic Co NNs, which induce more important Rh moments. One concludes that the chemical order, the resulting shape of the interfaces, and the possible interactions with the surface play a central role in the magnetic behavior of nanoalloys.

IV. CONCLUSION

The magnetic properties of core-shell CoRh nanoparticles have been investigated systematically in the framework of density-functional theory. The role of exchange and correlation effects on the magnetism of these clusters has been explored by comparing the results obtained using the spin-polarized LDA and GGA functionals. The importance of the chemical order on the magnetic behavior has been quantified and analyzed. This concerns, on the one side, interesting proximity effects between magnetic and nonmagnetic elements, which are similar to what has been already observed in bulk magnetic alloys. Let us mention, for example, the development of significant local spin moments in otherwise paramagnetic elements, and the strong dependence of these induced moments on the local concentration of magnetic atoms around a nonmagnetic elements (e.g., Co concentration around Rh). In addition, specific finite-size effects associated to the reduction of size, to the changes in local coordination numbers, and to the interplay between surface, interface, and bulklike local environments have been observed. All considered Co_xRh_{1-x} clusters having $N = 43$ and $N = 273$ atoms are found to be magnetic with an average spin moment per CoRh unit that is larger than in CoRh macroscopic alloys with similar concentrations. This is mainly the consequence of two contributions: an enhancement of the Co moments and important induced spin moments at the Rh atoms, which couple parallel to the Co moments. Moreover, the latter show a nontrivial dependence of the distance to the interface, particularly due to charge transfers from Co to Rh atoms. In addition, we have correlated the local magnetic moments to the corresponding electronic densities of states, which reflect the dependence of the cluster electronic structure on concentration and chemical order. The properties of CoRh interfaces and the effects of coating $3d$ clusters with $4d$ shells, and vice versa, have been quantified. A particularly interesting future research direction is to investigate the magnetic anisotropy energy of these nanoalloys as a function of Rh concentration, since it is relevant for potential applications. Furthermore, multiaxial magnetoanisotropic behaviors, leading to a complex magnetization reversal process, are likely to occur depending on composition and chemical order. Finally, the contributions of orbital magnetism and the correlations between orbital moments and magnetic anisotropy deserve to be explored in more detail from a first-principles perspective.

ACKNOWLEDGMENTS

It is a pleasure to thank Dr. P. Ruiz-Díaz for helpful discussions and useful comments. This work has been supported in part by CONACyT Grants No. 62292 and No. 182290, the Deutsche Forschungsgemeinschaft, the DAAD-CONACyT exchange program PROALMEX, and the COST Action MP0903 on Nanoalloys. Computer resources were provided by the IT Service Center of the University of Kassel, the Center for Scientific Computing of the University of Frankfurt, and the John von Neumann Institute for Computing. One of the authors (L.E.D.S.) has been a postdoctoral fellow of the Deutscher Akademischer Austausch Dienst. The technical support from J. Rentería and J. C. Sánchez is gratefully acknowledged.

[1]See, for instance, *Nanomagnetism*, edited by D. L. Mills and J. A. C. Bland (Elsevier, Amsterdam, 2006).
[2]S. Sun, C. B. Murray, D. Weller, L. Folks, and A. Moser, Science **287**, 1989 (2000).
[3]J. Bansmann, S. H. Baker, C. Binns, J. A. Blackman, J.-P. Bucher, J. Dorantes-Dávila, V. Dupuis, L. Favre, D. Kechrakos, A. Kleibert, K.-H. Meiwes-Broer, G. M. Pastor, A. Perez, O. Toulemonde, K. N. Trohidou, J. Tuaillon, and Y. Xie, Surf. Sci. Rep. **56**, 189 (2005).
[4]R. Ferrando, J. Jellinek, and R. L. Johnston, Chem. Rev. **108**, 845 (2008).
[5]S. Yin, R. Moro, X. Xu, and W. A. de Heer, Phys. Rev. Lett. **98**, 113401 (2007); M. E. Gruner, G. Rollmann, P. Entel, and M. Farle, *ibid.* **100**, 087203 (2008); M. B. Knickelbein, Phys. Rev. B **75**, 014401 (2007); F. Tournus, A. Tamion, N. Blanc, A. Hannour, L. Bardotti, B. Prével, P. Ohresser, E. Bonet, T. Epicier, and V. Dupuis, *ibid.* **77**, 144411 (2008); S. Sahoo, A. Hucht, M. E. Gruner, G. Rollmann, P. Entel, A. Postnikov, J. Ferrer, L. Fernández-Seivane, M. Richter, D. Fritsch, and S. Sil, *ibid.* **82**, 054418 (2010).
[6]D. M. Cox, D. J. Trevor, R. L. Whetten, E. A. Rohlfing, and A. Kaldor, Phys. Rev. B **32**, 7290 (1985).
[7]K. Lee, J. Callaway, K. Kwong, R. Tang, and A. Ziegler, Phys. Rev. B **31**, 1796 (1985).
[8]W. A. de Heer, P. Milani, and A. Châtelain, Phys. Rev. Lett. **65**, 488 (1990); I. M. L. Billas, J. A. Becker, A. Châtelain, and W. A. de Heer, *ibid.* **71**, 4067 (1993); J. P. Bucher, D. C. Douglass, and L. A. Bloomfield, *ibid.* **66**, 3052 (1991); D. C. Douglass, A. J. Cox, J. P. Bucher, and L. A. Bloomfield, Phys. Rev. B **47**, 12874 (1993); M. B. Knickelbein, J. Chem. Phys. **125**, 044308 (2006).
[9]G. M. Pastor, J. Dorantes-Dávila, and K. H. Bennemann, Physica B **149**, 22 (1988); Phys. Rev. B **40**, 7642 (1989).
[10]R. A. Guirado-López, J. Dorantes-Dávila, and G. M. Pastor, Phys. Rev. Lett. **90**, 226402 (2003).
[11]G. M. Pastor, J. Dorantes-Dávila, S. Pick, and H. Dreyssé, Phys. Rev. Lett. **75**, 326 (1995).
[12]R. Galicia, Rev. Mex. Fis. **32**, 51 (1985); J. Dorantes-Dávila, H. Dreyssé, and G. M. Pastor, Phys. Rev. B **46**, 10432 (1992); B. V. Reddy, S. N. Khanna, and B. I. Dunlap, Phys. Rev. Lett. **70**, 3323 (1993); Yang Jinlong, F. Toigo, W. Kelin, and Zhang Manhong, Phys. Rev. B **50**, 7173 (1994); Yang Jinlong, F. Toigo, and W. Kelin, *ibid.* **50**, 7915 (1994); B. Piveteau, M-C. Desjonquéres, A. M. Olés, and D. Spanjaard, *ibid.* **53**, 9251 (1996); P. Villaseñor-González, J. Dorantes-Dávila, H. Dreyssé, and G. M. Pastor, *ibid.* **55**, 15084 (1997); L. Vitos, B. Johansson, and J. Kollar, *ibid.* **62**, R11957 (2000).
[13]A. J. Cox, J. G. Louderback, and L. A. Bloomfield, Phys. Rev. Lett. **71**, 923 (1993); A. J. Cox, J. G. Louderback, S. E. Apsel, and L. A. Bloomfield, Phys. Rev. B **49**, 12295 (1994).
[14]T. Taniyama, E. Ohta, and T. Sato, Europhys. Lett. **38**, 195 (1997).
[15]D. Zitoun, M. Respaud, M-C. Fromen, M. J. Casanove, P. Lecante, C. Amiens, and B. Chaudret, Phys. Rev. Lett. **89**, 037203 (2002).
[16]M. Muñoz-Navia, J. Dorantes-Dávila, D. Zitoun, C. Amiens, N. Jaouen, A. Rogalev, M. Respaud, and G. M. Pastor, Appl. Phys. Lett. **95**, 233107 (2009).
[17]T. Sondón and J. Guevara, J. Magn. Magn. Mater. **272**, e1247 (2004); E. O. Berlanga-Ramírez, F. Aguilera-Granja, J. M. Montejano-Carrizales, A. Díaz-Ortiz, K. Michaelian, and A. Vega, Phys. Rev. B **70**, 014410 (2004).
[18]F. Tournus, K. Sato, T. Epicier, T. J. Konno, and V. Dupuis, Phys. Rev. Lett. **110**, 055501 (2013); N. Blanc, L. E. Díaz-Sánchez, A. Y. Ramos, F. Tournus, H. C. N. Tolentino, M. De Santis, O. Proux, A. Tamion, J. Tuaillon-Combes, L. Bardotti, O. Boisron, G. M. Pastor, and V. Dupuis, Phys. Rev. B **87**, 155412 (2013).
[19]R. Cuadrado and R. W. Chantrell, Phys. Rev. B **86**, 224415 (2012).
[20]C. Antoniak, M. E. Gruner, M. Spasova, A. V. Trunova, F. M. Römer, A. Warland, B. Krumme, K. Fauth, S. Sun, P. Entel, M. Farle, and H. Wende, Nat. Commun. **2**, 528 (2011).
[21]J. Dorantes Dávila and G. M. Pastor, in *Nanoalloys: From Fundamentals to Emergent Applications*, edited by F. Calvo (Elsevier, Amsterdam, 2013), Chap. 8.
[22]A. Oswald, R. Zeller, and P. H. Dederichs, Phys. Rev. Lett. **56**, 1419 (1986); H. Beckmann and G. Bergmann, *ibid.* **83**, 2417 (1999).
[23]P. Gambardella, S. Rusponi, M. Veronese, S. S. Dhesi, C. Grazioli, A. Dallmeyer, I. Cabria, R. Zeller, P. H. Dederichs, K. Kern, C. Carbone, and H. Brune, Science **300**, 1130 (2003).
[24]Muñoz-Navia, J. Dorantes-Dávila, D. Zitoun, C. Amiens, B. Chaudret, M.-J. Casanove, P. Lecante, N. Jaouen, A. Rogalev, M. Respaud, and G. M. Pastor, Faraday Discuss. **138**, 181 (2008).
[25]S. Dennler, J. L. Ricardo-Chávez, J. Morillo, and G. M. Pastor, Eur. Phys. J. D **24**, 237 (2003); S. Dennler, J. Morillo, and G. M. Pastor, J. Phys.: Condens. Matter **16**, S2263 (2004); Surf. Sci. **532**, 334 (2003).
[26]J. Lv, F-Q. Zhang, X-H. Xu, and H-S. Wu, Chem. Phys. **363**, 65 (2009).
[27]P. Hohenberg and W. Kohn, Phys. Rev. **136**, B864 (1964); W. Kohn and L. J. Sham, *ibid.* **140**, A1133 (1965).
[28]G. Kresse and J. Furthmüller, Comput. Mater. Sci. **6**, 15 (1996).
[29]G. Kresse and J. Furthmüller, Phys. Rev. B **54**, 11169 (1996).
[30]G. Kresse and D. Joubert, Phys. Rev. B **59**, 1758 (1999).
[31]P. E. Blöchl, Phys. Rev. B **50**, 17953 (1994).
[32]U. von Barth and L. Hedin, J. Phys. C: Solid State Phys. **5**, 1629 (1972).
[33]S. H. Vosko, L. Wilk, and M. Nusair, Can. J. Phys. **58**, 1200 (1980).
[34]J. P. Perdew and Y. Wang, Phys. Rev. B **45**, 13244 (1992).
[35]J. P. Perdew, J. A. Chevary, S. H. Vosko, K. A. Jackson, M. R. Pederson, D. J. Singh, and C. Fiolhais, Phys. Rev. B **46**, 6671 (1992).
[36]N. D. Mermin, Phys. Rev. **137**, A1441 (1965); A. De Vita, Ph.D. thesis, Keele University, 1992; A. De Vita and M. J. Gillan, J. Phys.: Condens. Matter **3**, 6225 (1991).
[37]H. J. Monkhorst and J. D. Pack, Phys. Rev. B **13**, 5188 (1976).
[38]K. Schwarz and P. Mohn, J. Phys. F: Met. Phys. **14**, L129 (1984).
[39]R. Singh and P. Kroll, Phys. Rev. B **78**, 245404 (2008).
[40]The fact the energy $E(S_z)$ obtained in DFT calculations based on the spin-polarized LDA or GGA is not independent of S_z for $|S_z| \leqslant S$, where S refers to the ground state total spin—as required by the spin-rotational invariance of the nonrelativistic Hamiltonian—is not a limitation in this context, since we are interested in the ground-state behavior. In general we find that E first decreases slowly with increasing S_z for $0 \leqslant S_z \leqslant S$, as already observed in Ref. 39, and then shows a more or less sharp increase at $S_z = S + 1$. It is actually this last energy increase, which allows us to identify rigorously the ground-state value of S, since states having $S_z \geqslant S + 1$ are necessarily orthogonal to those having a total spin $S' \leqslant S$. The calculated increment of E for $S_z < S$ seems to be an artifact of the LDA or GGA, which can be interpreted as the result of mixtures

between the ground state and higher-energy states having the same S_z but lower total spin.

[41] M. P. Teter, M. C. Payne, and D. C. Allan, Phys. Rev. B **40**, 12255 (1989).

[42] D. M. Bylander, L. Kleinman, and S. Lee, Phys. Rev. B **42**, 1394 (1990).

[43] B. V. Reddy, S. K. Nayak, S. N. Khanna, B. K. Rao, and P. Jena, Phys. Rev. B **59**, 5214 (1999).

[44] A. Kant and B. Strauss, J. Chem. Phys. **41**, 3806 (1964).

[45] D. A. Hales, C.-X. Su, L. Lian, and P. B. Armentrout, J. Chem. Phys. **100**, 1049 (1994).

[46] D. Fritsch, K. Koepernik, M. Richter, and H. Eschrig, J. Comp. Chem. **29**, 2210 (2008).

[47] Y-Ch. Bae, V. Kumar, H. Osanai, and Y. Kawazoe, Phys. Rev. B **72**, 125427 (2005).

[48] C. Kittel, *Introduction to Solid State Physics*, 7th ed. (Wiley, New York, 1996).

[49] Z.-Q. Li, Y. Hashi, J.-Z. Yu, K. Ohno, and Y. Kawazoe, J. Phys.: Condens. Matter **7**, 7367 (1995).

[50] Z.-Q. Li, J.-Z. Yu, K. Ohno, and Y. Kawazoe, J. Phys.: Condens. Matter **7**, 47 (1995).

[51] J. H. Mokkath and G. M. Pastor, Phys. Rev. B **85**, 054407 (2012); J. Phys. Chem. C **116**, 17228 (2012).

[52] M. C. Fromen, J. Morillo, M.-J. Casanove, and P. Lecante, Europhys. Lett. **73**, 885 (2006).